

# Self-Unwrapping Phase-Shifting for Fast and Accurate 3-D Shape Measurement

Jinghui Zeng<sup>1</sup>, Wenxin Ma<sup>1</sup>, Wei Jia<sup>1</sup>, Yucheng Li<sup>1</sup>, Haowen Li<sup>1</sup>,  
Xuewen Liu<sup>1</sup>, and Mingkui Tan<sup>1</sup>, *Member, IEEE*

**Abstract**—Phase unwrapping is one of the most important procedures in 3-D phase measurement profilometry (PMP) and has attracted great research interest in the past few decades. However, the existing phase unwrapping methods require additional patterns or preassumptions to determine the fringe orders for further absolute phase retrieval, which dramatically affect the measurement efficiency. To address this problem, we propose a generic self-unwrapping phase-shifting (SUPS) algorithm that retrieves the absolute phase without external information or priors. To this end, we first embed a novel space-varying phase shift (SPS) that uniquely determines the fringe order information into sinusoidal patterns, and then extract it to retrieve the absolute phase by pixelwise calculation. Our method achieves higher efficiency over previous methods while preserving the measurement precision, and the minimum number of patterns required is only four. All the theoretical, simulation, and extensive experimental results demonstrate its superiority in fast and accurate 3-D shape measurement.

**Index Terms**—3-D shape measurement, fringe projection profilometry, phase measurement profilometry (PMP), phase unwrapping, structured light.

## I. INTRODUCTION

PHASE measurement profilometry (PMP) has been an active research area in 3-D shape measurement and extensively used in industrial fields such as quality control and defect detection [1]–[4]. The main idea of PMP approaches is to project periodical fringe pattern(s) and establish accurate

correspondences through phase information. However, the periodical nature of PMP patterns results in a phase ambiguity problem where the extracted phase is wrapped within  $2\pi$  with disconnections. Therefore, restoring the absolute phase, also known as phase unwrapping, becomes an indispensable process to establish unique correspondences [5], [6]. Besides, phase unwrapping is also an indispensable component in synthetic aperture radar interferometry, magnetic resonance imaging, and optical interferometry [7].

In the past few decades, many phase unwrapping methods have been proposed [8]–[12]. These phase unwrapping approaches can be divided into two categories: spatial phase unwrapping and temporal phase unwrapping [11]. The spatial phase unwrapping methods assume that the measured surface is continuous, and hence the absolute phase can be obtained through local [13], [14] or global optimization [15]–[17]. However, the error propagation problem would induce continuous artifacts and it is always challenging to handle complex surfaces with large disconnections for such methods [18], [19].

The temporal phase unwrapping methods project additional patterns for absolute phase retrieval. One of the most representative methods is multifrequency phase-shifting (MFPS) [20]–[24] that projects extra phase-shifting patterns with various frequencies and retrieves the absolute phase through two or more wrapped phase maps. Many hybrid methods have also been developed that use extra patterns to straightforwardly provide fringe order information, such as Gray-code [25], color coding [26], and phase coding strategies [27]–[29]. Temporal phase unwrapping methods are more robust to complex measurement scenarios and thus widely used in real-world applications. However, the extra pattern projections dramatically decrease the measurement efficiency.

To improve the efficiency of phase unwrapping, some embedding-based approaches have been developed. These methods address the phase ambiguity problem by embedding recognizable intensity signals, such as pseudorandom speckle [30], [31], f1 noise [32], or triangular wave [33]. These methods are easy to implement in PMP systems, but the embedded intensity signals are sensitive to surface reflectivity variations and lens defocusing [34]. Recently, Wu *et al.* [35] proposed a high-resolution few-pattern method that uses only four patterns for 3-D measurement. Subsequently, Wu *et al.* [36] further proposed an inner shifting phase method for high-speed measurement. The shared idea behind these two methods [35], [36] is to encode the fringe order information into four specially designed patterns and hence obtain the wrapped phase and fringe orders simultaneously. Though improving

Manuscript received 18 February 2022; revised 8 May 2022; accepted 3 June 2022. Date of publication 4 July 2022; date of current version 25 July 2022. This work was supported in part by the National Natural Science Foundation of China (NSFC) under Grant 62072190, in part by the Key Realm Research and Development Program of Guangzhou under Grant 202007030007, and in part by the Program for Guangdong Introducing Innovative and Entrepreneurial Teams under Grant 2017ZT07X183. The Associate Editor coordinating the review process was Dr. Donghoon Kang. (*Corresponding author: Mingkui Tan.*)

Jinghui Zeng is with the Shien-Ming Wu School of Intelligent Engineering and the School of Software Engineering, South China University of Technology, Guangzhou 511442, China, and also with the Pazhou Laboratory, Guangzhou 510335, China (e-mail: z.jh11@mail.scut.edu.cn).

Wenxin Ma is with the School of Software Engineering, South China University of Technology, Guangzhou 510006, China (e-mail: 461562644@qq.com).

Wei Jia is with Guangzhou Shiyuan Electronic Technology Company, Ltd. (CVTE) Research, Guangzhou 510530, China (e-mail: jiawei@cvte.com).

Yucheng Li, Haowen Li, and Xuewen Liu are with the College of Electrical and Information Engineering, Hunan University, Changsha 410082, China (e-mail: 707998032@qq.com; lihaowenhowan@163.com; liuxuewen19@hnu.edu.cn).

Mingkui Tan is with the School of Software Engineering and the Key Laboratory of Big Data and Intelligent Robot, Ministry of Education, South China University of Technology, Guangzhou 510006, China (e-mail: mingkuitan@scut.edu.cn).

Digital Object Identifier 10.1109/TIM.2022.3186705

the measurement efficiency, these methods can be sensitive to random noise and gamma distortion since only four patterns can be used. Also, our research has found that the encoded fringe order may lead to low phase quality in certain regions. These drawbacks limit their measurement performance and further application in more measurement scenarios.

Inspired by the success of deep learning techniques [37], many learning-based phase analysis methods have been developed. These methods take a single frame and determine the absolute phase [38], [39] or some intermediate results [40], [41]. These methods outperform traditional methods in many conditions; however, they require a large amount of training data, and the feasibility in scenes with large discontinuity or continuity artifacts is still an open question [41].

Although the above methods can restore the absolute phase, they are often designed for either high precision or high efficiency, ignoring that a good trade-off between precision and efficiency is important in real-world measurement. In this work, we seek to achieve high precision and high efficiency simultaneously. Our method is inspired by the embedding-based methods [35], [36], which are quite efficient since they are very promising for reducing the number of patterns projected. Unfortunately, the precision of these methods remains to be improved.

To address this limitation, we propose a generic self-unwrapping phase-shifting (SUPS) method that does not require extra patterns. Unlike traditional methods where all fringe pixels share a phase shift, we introduce a novel space-varying phase shift (SPS) that varies with the pixel coordinates and uniquely determines the fringe orders. By introducing a sign function, we embed the SPS into sinusoidal fringes, from which the wrapped phase and fringe order can be extracted simultaneously. The SUPS method is a generic multistep phase-shifting method, and the shifting step can be freely set according to the efficiency and accuracy requirements. Our main contributions are summarized as follows.

- 1) We propose an SUPS method that requires no additional patterns, and the minimum number of patterns required is only four. In addition, our study has demonstrated that SPS is open, indicating its extensibility to more coding strategies.
- 2) We demonstrate the superiority of the SUPS method over the conventional phase-shifting methods theoretically. To the best of our knowledge, this is the first time the error model of the SUPS method is established, providing theoretical guidelines for practical applications.
- 3) All extensive simulations and practical comparative experiments demonstrate its feasibility and superiority in fast and accurate 3-D shape measurement.

The remainder of this article is as follows. Section II discusses the principle and theoretical analysis. Section III describes the simulation results. Section IV shows the real-world shape measurement results and discusses the effectiveness of the proposed method. Section V concludes this work.

## II. PRINCIPLE

### A. Multifrequency Phase-Shifting Algorithm

The basic idea of phase-shifting methods is to introduce a time-varying phase shift (TPS) into sinusoidal fringe pattern

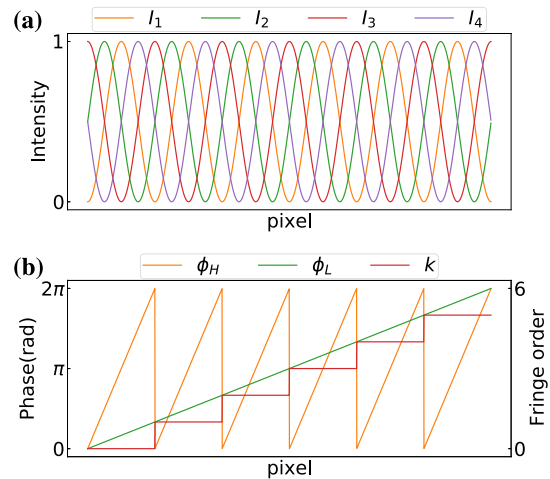


Fig. 1. Principle of the four-step MFPS method. (a) Cross section of four high-frequency sinusoidal fringes. (b) Extracted phase corresponding to two frequencies and the obtained fringe order.

sequences. Generally, the intensity of  $N$ -step phase-shifting patterns can be mathematically described as

$$I_n^p(x, y) = A^p + B^p \cos[\Phi(x, y) + \delta_n] \quad (1)$$

where the superscript  $p$  denotes the projector,  $n$  is the pattern index, and  $n = 0, 1, \dots, N - 1$ , and  $A$  and  $B$  denote the intensity bias and intensity modulation, respectively. Here,  $\Phi(x, y) = 2\pi x/\lambda$  is the sinusoidal phase and  $\lambda$  denotes the fringe period or the fringe wavelength, with the unit of pixels. Note that since we use vertical fringes, the phase increases with the  $x$ -coordinate and  $\delta_n$  denotes the time-varying phase shift. Apparently, three patterns are the minimum number of patterns required to determine these three unknowns in (1). But in real-world applications, more than three patterns are commonly used to compress the inevitable noise, and hence the phase is determined through the least-square algorithm [18], [34]. Specifically, if the phase shift  $\delta_n$  is equal and in the form of

$$\delta_n = 2\pi n/N, \quad n = 0, 1, \dots, N - 1 \quad (2)$$

simultaneously solving these  $N$  equations leads to

$$\phi(x, y) = -\tan^{-1} \frac{\sum_{n=0}^{N-1} I_n^p(x, y) \sin \delta_n}{\sum_{n=0}^{N-1} I_n^p(x, y) \cos \delta_n} + \pi. \quad (3)$$

Fig. 1(a) shows the cross sections of the typical four-step phase-shifting fringe patterns. As can be seen, these fringes are sinusoidal and shifted equally corresponding to the pattern index. Limited by the arc-tangent function, the extracted phase using (3) is wrapped in  $[0, 2\pi)$  with  $2\pi$  disconnections.

The phase unwrapping procedure removes these disconnections by adding integer multiples of  $2\pi$ , and the integer is referred to as the fringe order  $k$ . Mathematically, the unwrapped phase can be expressed as

$$\Phi(x, y) = \phi(x, y) + 2\pi k(x, y). \quad (4)$$

The MFPS algorithm determines the fringe order by one (or more) extra wrapped phase map(s) obtained from patterns with lower frequencies. Taking two wrapped phase

maps  $\phi_H$  and  $\phi_L$  corresponding to high and low frequencies, respectively, where  $\phi_L$  is a unit-frequency phase ranging between  $[0, 2\pi)$ , then the fringe order can be determined by

$$k = \text{round}\left[\frac{\phi_L(\lambda_L/\lambda_H) - \phi_H}{2\pi}\right] \quad (5)$$

where  $\lambda_H$  and  $\lambda_L$  are the fringe periods corresponding to high and low frequencies, respectively,  $\text{round}(\cdot)$  function returns the nearest integer pixel intensity, and the pixel coordinate is omitted. A simplified principle of phase unwrapping is illustrated in Fig. 1(b), and more details can be referred to [6]. As (4) suggests, since the unit-frequency patterns only provide the fringe order, the unwrapped phase and the final measurement accuracy depend primarily on the high-frequency patterns. However, the unit-frequency patterns double the total projection number and dramatically affect the measurement efficiency.

### B. Self-Unwrapping Phase-Shifting Algorithm

The conventional MFPS methods suffer from additional pattern projections, while in the SUPS method, we remove the redundant patterns by embedding an extra SPS. The SPS, as the name suggests, varies with the pixel coordinates and is marked as  $\alpha(x, y)$ . Therefore, the phase shift in the SUPS patterns consists of two parts: the conventional time-varying phase shift  $\delta_n$  and the SPS  $\alpha(x, y)$ . According to the discussions in Section I, the SPS coding function should meet the following requirements.

- 1) *Contrast-Preserve*: To preserve the accuracy, the SPS should not affect the fringe amplitude or the contrast.
- 2) *Ambiguity-Free*: The SPS should uniquely determine the fringe orders, indicating no ambiguity exists in the SPS.
- 3) *Extractability*: The SPS should be extractable to determine the fringe order and wrapped phase simultaneously.

For the contrast-preserve requirement, since the SPS is embedded in the phase of sinusoidal fringes, the fringe amplitude is naturally preserved. To meet the ambiguity-free requirement, the SPS should be a single-valued function mathematically, e.g., a linear function or a uniform staircase function. In this article, we mainly discuss the linear function case in the form

$$\alpha(x, y) = Rx/S - R/2. \quad (6)$$

Here,  $R$  denotes the SPS range that is less than  $2\pi$ , and  $S$  denotes the pattern pixel resolution in the  $x$ -direction. Note that the SPS cannot be embedded by simple addition or subtraction, which would make it hard to extract. To meet the requirement of extractability, we propose a specially designed embedding strategy with a time-varying sign function.

Specifically, the mathematical expression of the SUPS patterns is as follows:

$$I_n^p(x, y) = A^p + B^p \cos[2\pi x/\lambda + \delta_n + \alpha(x, y) \cdot s_N(n)] \quad (7)$$

where  $\delta_n$  denotes the equal TPS, and  $n = 0, 1, \dots, 2N - 1$ . Here,  $s_N(n)$  denotes the time-varying sign function

$$s_N(n) = \begin{cases} -1, & n < N \\ 1, & n \geq N. \end{cases} \quad (8)$$

This sign function is essential for decoupling the sinusoidal phase and the SPS, without which the phase and the SPS are not splittable. These projected patterns are distorted by the surface geometry and can be expressed as

$$I_n^c(x, y) = A^c + B^c \cos[\Phi(x, y) + \delta_n + \alpha(x, y) \cdot s_N(n)] \quad (9)$$

where  $A^c$  and  $B^c$  denote the average intensity and intensity modulation in the captured images, respectively. Since both phase decoding and unwrapping are pixelwise calculations, we omit the coordinate  $(x, y)$  and the superscript for simplicity in the following. We determine the wrapped phase and fringe orders separately. Specifically, for the wrapped phase  $\phi$ , simultaneously solving (9) leads to

$$\phi = -\tan^{-1}\left(\frac{K_1}{K_2}\right) + \pi \quad (10)$$

with

$$\begin{cases} K_1 = \sum_{n=0}^{2N-1} I_n \sin \delta_n = NB \sin \Phi \cos \alpha \\ K_2 = \sum_{n=0}^{2N-1} I_n \cos \delta_n = NB \cos \Phi \cos \alpha. \end{cases} \quad (11)$$

Note that all the projected patterns are used to determine the wrapped phase. When  $N$  is even, we extract the SPS as follows:

$$\alpha = \tan^{-1}\left(\frac{K_3}{K_4}\right) \quad (12)$$

with

$$\begin{cases} K_3 = \sum_{n=0}^{N-1} (I_n + I_{n+N}) s_{\frac{N}{2}}(n) = 2B \sin \alpha \sum_{n=0}^{N-1} \cos(\Phi - \delta_n) \\ K_4 = \sum_{n=0}^{N-1} (I_n - I_{n+N}) = 2B \cos \alpha \sum_{n=0}^{N-1} \cos(\Phi - \delta_n). \end{cases} \quad (13)$$

Also,  $s_{(N/2)}(n)$  is a time-dependent sign function

$$s_{\frac{N}{2}}(n) = \begin{cases} -1, & n < \frac{N}{2} \\ 1, & n \geq \frac{N}{2}. \end{cases} \quad (14)$$

When  $N$  is odd, a constant coefficient needs to be multiplied

$$\alpha = \tan^{-1}\left[\frac{\sum_{n=1}^{N-1} (I_n + I_{n+N}) s_{\frac{N}{2}}(n)}{\sum_{n=1}^{N-1} (I_n - I_{n+N})} \cdot \frac{-\sum_{n=1}^{N-1} \sin \delta_n}{\sum_{n=1}^{N-1} s_{\frac{N}{2}}(n) \cos \delta_n}\right]. \quad (15)$$

Here, we omit  $I_0$  and  $I_N$  to eliminate the intensity bias  $A$  in the derivation. Fig. 2 shows how the SUPS method simultaneously determines the wrapped phase and the fringe order. Fig. 2(a) shows the cross sections of four-step SUPS fringes. Unlike the conventional phase-shifting methods, the SUPS fringes are not equally shifted sinusoidal fringes. In essence, the SPS destroys

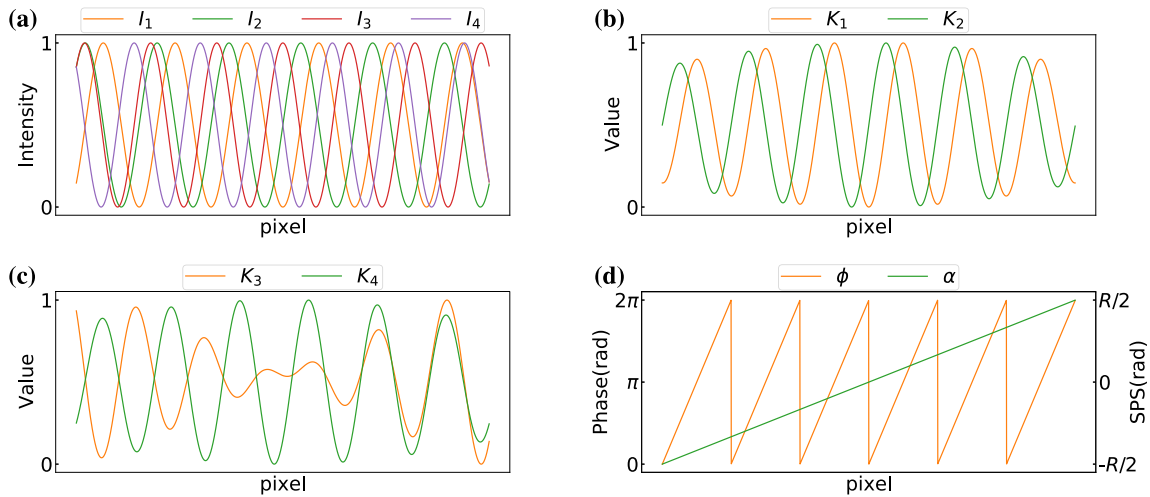


Fig. 2. Principle of the SUPS method. (a) Cross section of four SUPS fringes. Note that the phase shift is no longer equal but varies with pixel coordinate. Intermediate results of (b) phase extraction and (c) SPS extraction. (d) Extracted wrapped phase and SPS.

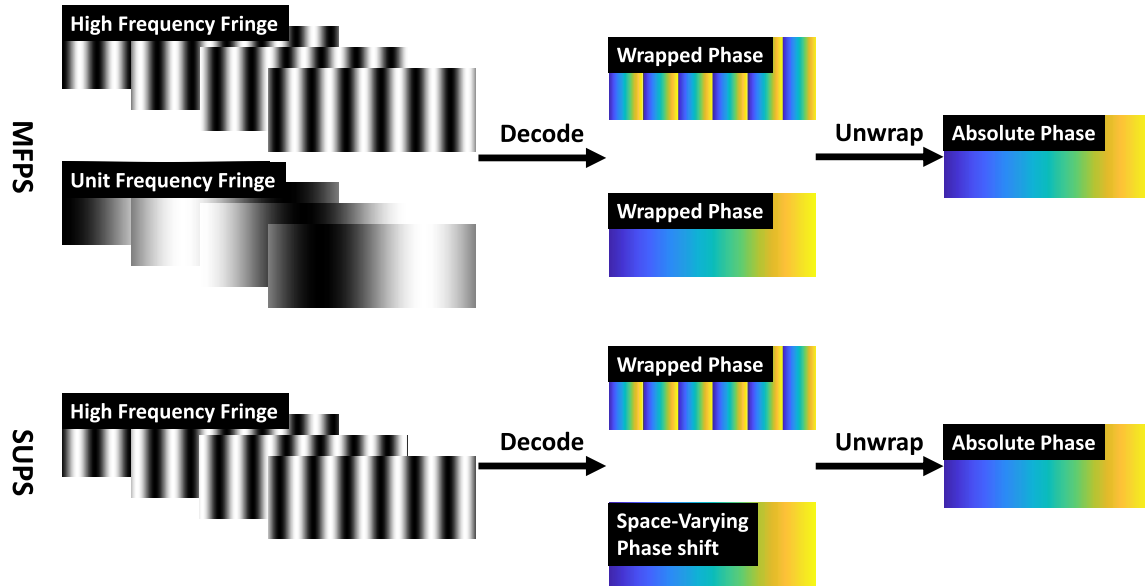


Fig. 3. Overall schematic. Top: MFPS approaches use additional fringes to determine the absolute phase. Bottom: SUPS method determines the wrapped phase and fringe order simultaneously.

the periodicity of fringes to carry fringe order information. Fig. 2(b) and (c) shows the intermediate results corresponding to (10) and (12) during the phase extraction process, and Fig. 2(d) shows the wrapped phase and SPS extracted from Fig. 2(c) and (d). Compared with Fig. 1, it is apparent that the extracted SPS can also be treated as a unit-frequency phase, but the major difference lies in that it is embedded in the high-frequency patterns internally rather than extracted from additional patterns. Since the extracted SPS ranges from  $-R/2$  to  $R/2$  monotonically without ambiguity, we determine the fringe order  $k$  similarly by

$$k = \text{round} \left[ \frac{(2\pi \alpha / R + \pi)(S/\lambda) - \phi}{2\pi} \right] \quad (16)$$

where  $S$  and  $\lambda$  are the pattern pixel resolution in (6) and the fringe period in (7), respectively. Given the wrapped phase  $\phi(x, y)$  and fringe order  $k(x, y)$ , we determine the absolute phase straightforwardly by (4).

Comparing (1) and (7), in essence our proposed SUPS explicitly encodes the fringe order information as the fourth unknown. Therefore, we do not need extra patterns to provide the fringe order information, which leads to dramatic efficiency improvement. Moreover, the four unknown (7) means we only need at least four patterns to determine the wrapped phase and the fringe order, while the conventional MFPS requires at least six patterns. The overall difference between SUPS and MFPS is illustrated in Fig. 3.

### C. Theoretical Analysis

In this section, we analyze how noise affects the measurement performance and compare it with the widely used MFPS approaches. We also discuss how to select the fringe parameters (e.g., the frequency, the SPS range) to achieve higher measurement performance.

Many existing phase-shifting profilometry studies [6] have demonstrated that when the image noise is a

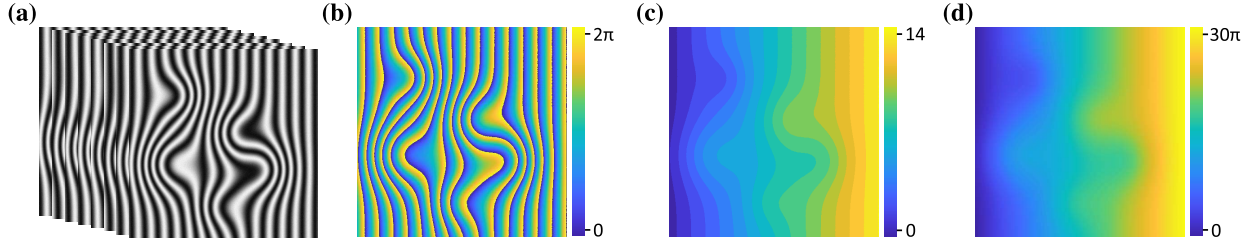


Fig. 4. Simulation results. (a) Deformed SUPS fringes. (b) Wrapped phase map. (c) Corresponding fringe orders. (d) Retrieved absolute phase distribution from (b) and (c).

Gaussian-distributed additive noise with a variance of  $\sigma_I^2$ , the extracted phase error variance can be expressed as

$$\sigma_\phi^2 = \frac{2\sigma_I^2}{Nf^2B^2} \quad (17)$$

where  $N$ ,  $f$ , and  $B$  denote the phase-shifting step, the fringe frequency, and the captured fringe modulation, respectively. According to Section II-A, the measurement error for an MFPS system depends primarily on the projected highest frequency patterns; however, it should be noted that the projection of the non-highest frequency patterns also takes time and affects the measurement efficiency. Therefore, we take the total projection number into consideration to evaluate the measurement efficiency. Without loss of generality, we define the percentage of patterns used to determine the phase as pattern utilization rate  $\eta$ . For example, the utilization rate is 50% for two-frequency phase-shifting and 33% for three-frequency phase-shifting. We denote the total projection number as  $M$ , then (17) is substituted to

$$\sigma_{\phi MF}^2 = \frac{1}{M\eta} \frac{2\sigma_I^2}{f^2B^2}. \quad (18)$$

To evaluate the phase error of the proposed SUPS, we similarly assume the noise is Gaussian-distributed and the variance is  $\sigma_I^2$ . According to the law of error propagation, we obtain the variance of phase error as

$$\sigma_{\phi SU}^2 = \sum \left[ \left( \frac{\partial \phi}{\partial I_n} \right)^2 \sigma_{I_n}^2 \right]. \quad (19)$$

Substituting (7) and (10) into (19), we obtain

$$\begin{aligned} \sigma_{\phi SU}^2 &= \sum \left[ \left( \frac{2}{M B \cos \alpha} \cos \left( \phi - \frac{2\pi n}{M} \right) \right)^2 \sigma_{I_n}^2 \right] \\ &= \frac{1}{M \cos^2 \alpha} \frac{2\sigma_I^2}{f^2 B^2} \end{aligned} \quad (20)$$

where  $\alpha$  is the SPS. Note that the pattern utilization rate of SUPS is 100% and is ignored here. As (20) tells, the SPS  $\alpha$  has great influence on phase uncertainty. Though the uncertainty is space-varying with  $\alpha$ , we can determine its upper bound. For a reasonable SPS range (e.g.,  $\pi/3$ , where  $\alpha$  ranges from  $-\pi/6$  to  $\pi/6$ ), the upper bound of the phase uncertainty is always much smaller than that of the conventional MFPS methods under the same setup. Furthermore, since  $\cos^2 \alpha$  is consistently bigger than  $\eta$ , we can use fewer SUPS patterns (higher efficiency) to achieve lower measurement error (higher accuracy) than the traditional MFPS methods, demonstrating its superiority in fast and accurate 3-D shape measurement.

The encoding strategies proposed in [35] and [36] can be regarded as four-step special cases of our SUPS method with the SPS range of  $\pi$  (from  $-\pi/2$  to  $\pi/2$ ). However, according to (20), the phase error is very high in the marginal regions where  $|\alpha(x, y)|$  is close to  $\pi/2$ . The nonoptimal parameter selection in [35] and [36] would cause performance degradation.

### III. SIMULATION

#### A. Feasibility Evaluation

To verify the feasibility of the proposed SUPS, we conduct numerical simulations. We simulate eight-step SUPS patterns, which means eight patterns are used to recover the absolute phase. The  $n$ th pattern can be described as

$$I_n(x, y) = \text{round} \{ A^P + B^P \cos [2\pi x/\lambda + \delta_n + \alpha(x, y) \cdot s_N(n) + \mathcal{N}] \} \quad (21)$$

where  $A^P$  and  $B^P$  are both 127.5 for a simulated 8-bit camera, the pattern resolution is  $256 \times 256$ , and the sinusoidal period is set to 16 pixels. In the following simulations, we set the embedded SPS range to  $\pi/3$  (from  $-\pi/6$  to  $\pi/6$ ) unless otherwise mentioned. Without loss of generality, we add Gaussian noise  $\mathcal{N}$  with a variance of 5 to the pixel intensity. We quantize the projection patterns using the  $\text{round}(\cdot)$  function.

We simulate the retrieved phase  $\Phi(x, y)$  by repeatedly adding Gaussian signals with random variance and position to a reference phase, and the corresponding deformed fringes are illustrated in Fig. 4(a). We then use the proposed decoding principle to determine the absolute phase. Specifically, we have eight intensity values for each pixel to decode the wrapped phase and the fringe order simultaneously, and the results are shown in Fig. 4(b) and (c), respectively. We conduct median filtering on the SPS map to remove some unexpected noise. As can be seen in the final result illustrated in Fig. 4(d), the proposed SUPS is able to recover the distorted phase map. To evaluate the accuracy, we calculate the residual error between the theoretical and the recovered absolute phase, and the root mean square error (RMSE) is 0.02003 rad.

#### B. Cost-Effectiveness Comparison

As discussed in Section II-C, increasing the number of patterns used can improve the measurement accuracy, but reduce the measurement efficiency. For a practical PMP system, we always expect to achieve higher measurement accuracy using fewer patterns, i.e., higher cost-effectiveness.

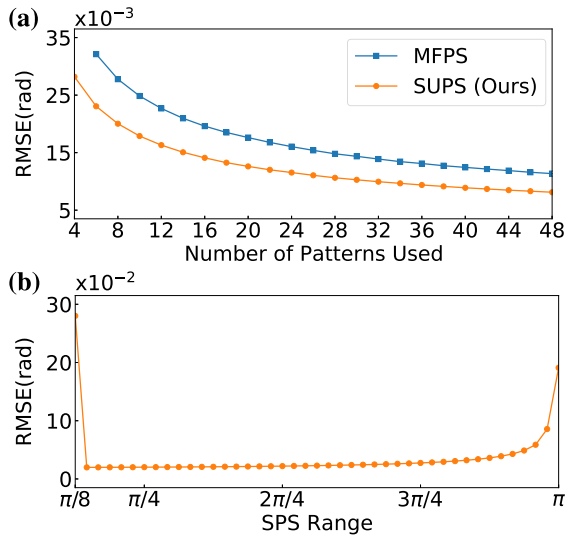


Fig. 5. Cost-effectiveness comparison. (a) Phase error (accuracy) versus the number of patterns used (efficiency). Note that the conventional MFPS method requires at least six patterns. (b) Phase error versus the SPS range.

To compare cost-effectiveness, we evaluate the phase error under different pattern numbers. For an intuitive comparison, we adopted a dual-frequency method, which also requires  $2N$  patterns for absolute phase calculation. We set the frequencies to 16 and 1, respectively, where the unit frequency is used to unwrap the high-frequency phase. We change the number of patterns used while keeping all the other settings consistent with those in Section III-A.

The simulation results illustrated in Fig. 5(a) are consistent with our intuition and (20). First, the minimum number of patterns is six for the conventional MFPS but four for SUPS. Second, as the number of patterns used increases, both SUPS and MFPS achieve higher performance. Third, when using equal patterns, the RMSE of our proposed SUPS is always less than that of the MFPS methods. Furthermore, it is noteworthy that the SUPS method achieves comparable performance using only half the patterns of MFPS. For example, the RMSE is 0.02003 rad for the eight-step SUPS while 0.01961 rad for the MFPS using 16 patterns. These results demonstrate that the proposed SUPS is more cost-effective than conventional TFPS.

We then discuss the influence of the SPS range on the phase error. As shown in Fig. 5(b), when the SPS range is greater than  $\pi/8$ , the phase error increases monotonically, and the curve becomes steeper as it approaches  $\pi$ . This phenomenon is consistent with what has been found in Section II-C that  $\sigma_{\phi S} \propto (1/(M)^{1/2} \cos \alpha)$ . Since the denominator at the marginal region is close to 0, the phase error increases sharply. Nevertheless, a smaller SPS range may not always lead to better results. It can be seen that when it is less than  $\pi/8$ , the error jumps by an order of magnitude. This is because the embedded SPS is too small to be extracted (e.g., close to 0), and the fringe order cannot be determined correctly, resulting in phase unwrapping failure. The error curve may vary with the noise level in real-world applications, but in general, we recommend setting the phase shift range between  $\pi/4$  and  $3\pi/4$ .

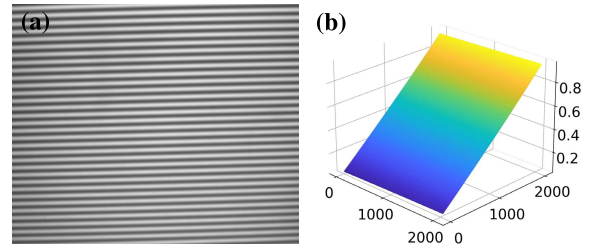


Fig. 6. Standard plane measurement result. (a) One of the capture of this plane. (b) Corresponding absolute phase.

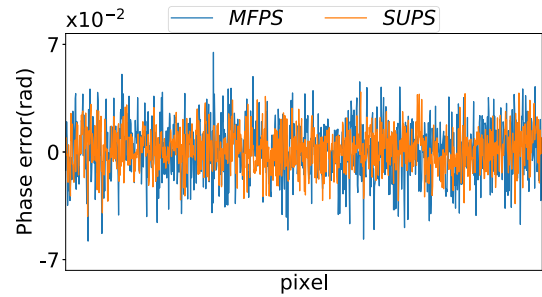


Fig. 7. Cross section of the phase error using two methods.

## IV. EXPERIMENTS AND DISCUSSION

### A. Experiment Setup

To verify the feasibility of the proposed SUPS in real-world 3-D shape measurement, we develop a structured light prototype system with an off-the-shelf digital light processing (DLP) projector (model: Texas Instruments LightCrafter 4500,  $912 \times 1140$  resolution, emission of 405-nm wavelength) and an 8-bit CMOS camera (model: FLIR BFLY-PGE-20S5M-C,  $2448 \times 2048$  resolution). To maximize the system depth of field (DOF), we placed the camera and the projector at  $30^\circ$ . The field of view of this system is about  $3 \text{ cm} \times 4.5 \text{ cm}$ .

To generate SUPS fringes, we set the phase-shifting step to 8 and the fringe frequency to 36 throughout the experiments, and the SPS range is  $\pi/3$  (from  $-\pi/6$  to  $\pi/6$ ) unless otherwise specified. We apply median filtering on the extracted SPS map to eliminate unexpected peaks and then use the filtered SPS map to unwrap the extracted wrapped phase. Finally, we calculate 3-D point clouds using the system calibration parameters using Zhang's method [42] and reconstruct the surfaces in MeshLab [43] for visualization.

### B. Performance Comparison

We first measure a white standard plane to evaluate the measurement accuracy. We place this plane vertically 130 mm in front of the camera lens and use the conventional three-frequency 32-step phase-shifting method to retrieve the ground-truth absolute phase.

After that, we keep the measured plane still and apply the proposed method to project fringe patterns. One of the captured fringe images is shown in Fig. 6(a). These images then are used to determine the wrapped phase and the embedded SPS simultaneously, and the retrieved absolute phase is illustrated in Fig. 6(b). We also conduct the widely used three-frequency four-step phase-shifting method, which

TABLE I  
MEASUREMENT OF THE STANDARD PLANE

Method	SPS range	Required pattern	RMSE( $10^{-3}rad$ )
3-frequency 4-step MFPS	—	12	18.38
12-step SUPS	$\pi/3$	12	10.93
8-step SUPS	$\pi/3$	8	13.20
4-step SUPS	$\pi/3$	4	17.71
4-step SUPS	$\pi$	4	24.59

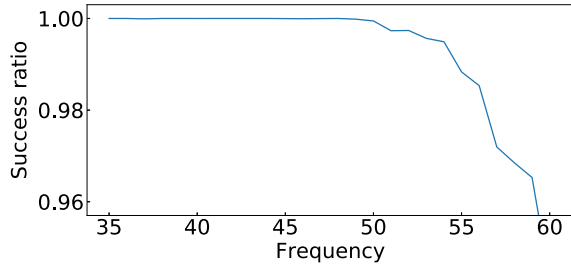


Fig. 8. Phase unwrapping success ratio versus fringe frequency for the SUPS method.

requires 12 patterns, to measure this plane and calculate the phase error. Fig. 7 shows the cross section of the absolute phase error for both the methods, and the RMSE for the three-frequency four-step phase-shifting (0.0184 rad) is 40% higher than that of the proposed method (0.0132 rad). It is clear that the proposed method achieves both higher measurement efficiency (fewer patterns) and higher accuracy (less phase error) than the conventional MFPS approaches.

We also evaluate the measurement performance under different fringe setups and list the results in Table I. As can be seen, when 12 patterns are used, the 12-step SUPS method achieves a much lower error (0.01093 rad) than the conventional MFPS method. This fits well with the theoretical analysis in Section II-C. However, what is in contrast to the expectations is that the four-step SUPS achieves even slightly better results (0.01771 rad) than the conventional method, which is contradictory to (18) and (20) that four-step SUPS should be inferior to the four-step phase-shifting method combined with the multifrequency phase unwrapping method. This phenomenon may be related to the additional low-frequency fringes in the traditional method, which is more sensitive to noise according to (18) and also introduces noise in the phase unwrapping procedure. However, when we set the SPS range to  $\pi$  and keep other parameters unchanged, the phase error increases dramatically from 0.01771 to 0.02459 rad. All these results are consistent with the theoretical analysis and simulation results above. We recommend again that an appropriate SPS range should be no larger than  $3\pi/4$ .

We further conducted experiments to explore how the fringe frequency affects the fringe order robustness. We keep the SPS range constant to  $\pi/3$  and change the fringe frequency, which means  $\pi/3$  is used to mark different numbers of fringes. We calculate whether the fringe order can be extracted successfully at different frequencies and plot the unwrapping success rate in Fig. 8. The experiment suggests that the

unwrapping success rate decreases as the fringe frequency increases. The reason is that increasing the fringe frequency is equivalent to decreasing the SPS range in Section III-B to some degree. The phase shift per fringe goes down under both the cases, and hence phase unwrapping is more likely to fail. The experimental result is consistent with the simulation, indicating that the fringe frequency and the SPS range are both affecting the unwrapping success rate.

### C. Real-World 3-D Shape Measurement

We also carry out more practical measurements in addition to the standard plane experiments. Real-world 3-D shape measurements are much more complicated, and it is always challenging for optical measurement techniques to handle complex surfaces with drastic changes in geometry, reflectivity variations, and isolated regions.

We first apply the proposed method to a sculpture as shown in Fig. 9(a). The size of the sculpture is approximately 50 mm  $\times$  40 mm  $\times$  30 mm and it is placed 130 mm in front of the camera. Fig. 9(b) shows one of the captured distorted patterns, and Fig. 9(c) shows the region of interest (ROI) mask. The second column in Fig. 9 shows how the wrapped phase is extracted, where Fig. 9(d) and (e) are the intermediate results  $K_1$  and  $K_2$ , and Fig. 9(f) is the corresponding wrapped phase. The third column shows how the SPS map is extracted, where Fig. 9(g) and (h) are the intermediate results  $K_3$  and  $K_4$ , and Fig. 9(i) is the corresponding SPS map (normalized). The wrapped phase and SPS are then used to determine the fringe order as shown in Fig. 9(j), which is further used for absolute phase retrieval and the result is shown in Fig. 9(k). Fig. 9(l) shows the reconstructed surface. As can be seen, the face and hair details are well-preserved. In addition, we carry out more measurement as shown in Fig. 10 to demonstrate its feasibility in complex surface measurement. These results indicate that the proposed method is reliable in measuring objects with complex surfaces.

We then compared the SUPS method with other embedding-based methods [35], [36] through practical measurements. We set the phase-shifting step to 4 and the SPS range to  $\pi/3$  for our SUPS method. The 32-step three-frequency phase shift method is used to obtain the ideal absolute phase in Fig. 11(a), then we calculate the phase errors of these methods, and show the results in Fig. 11(b)–(d). As can be seen, our SUPS method achieves better performance than the others. The inner shifting phase method [36] achieves comparable accuracy in the center region, but the phase error in the

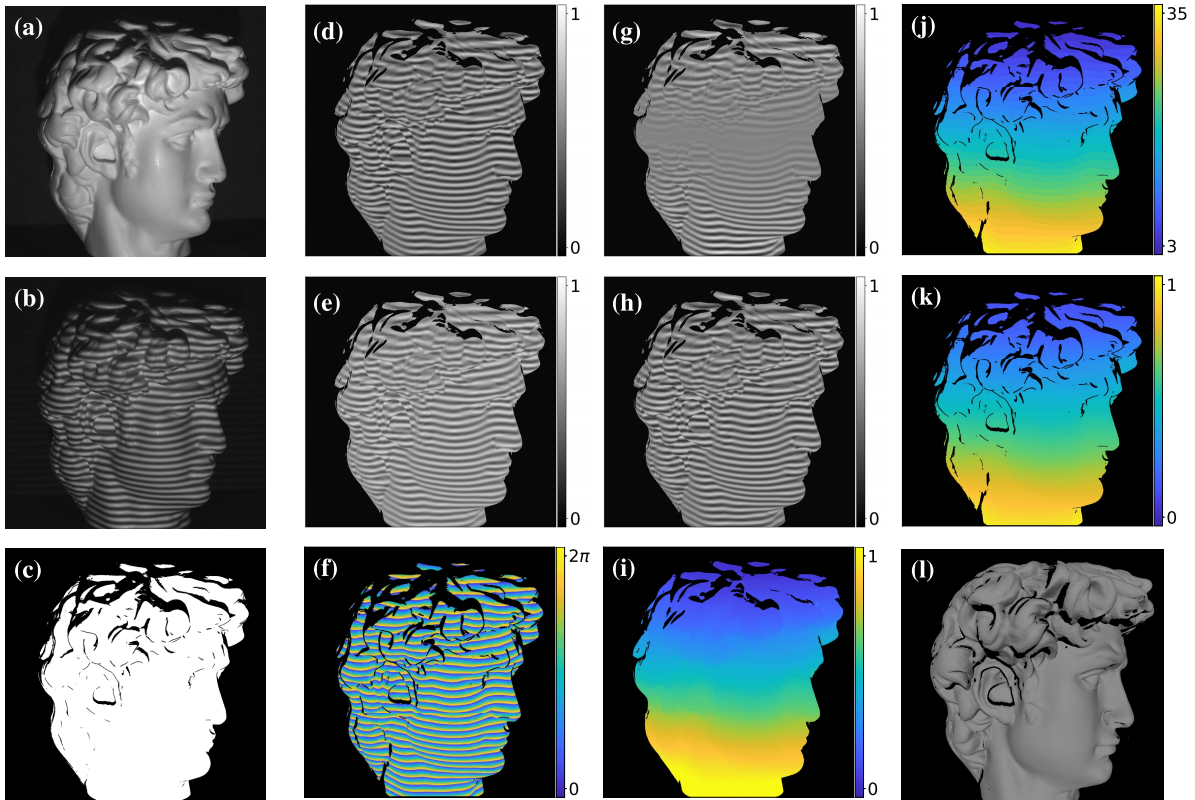


Fig. 9. Measurement result of the sculpture. (a) Photography of the sculpture. (b) One of the captured fringe patterns. (c) Intensity mask. Normalized intermediate results (d)  $K_1$  and (e)  $K_2$ . (f) Wrapped phase extracted using (d) and (e). Normalized intermediate results (g)  $K_3$  and (h)  $K_4$ . (i) Normalized SPS map extracted using (g) and (h). (j) Fringe order map. (k) Retrieved absolute phase (normalized). (l) Reconstructed surface.



Fig. 10. More experimental results on real-world complex surfaces. (a) and (b) Photograph of the measured sculptures. (c) and (d) Reconstructed surfaces.

top and the bottom regions increases abnormally. The phase error of [35] is similar to [36], but appears to be period-associated. We plot the cross section in Fig. 12 for better observation. As we declared in Section II, [35] and [36] are both special cases of the proposed SUPS, and hence the theoretical analysis in Section II-C can also be applied here. Specifically, [36] can be regarded as a four-step SUPS with the SPS range of  $\pi$ ; however, setting the SPS range to  $\pi$  increases the phase error in the side regions. Wu *et al.* [35]

further replace the linear SPS in [36] with discrete codewords (i.e., the fringe orders), which destroys the fringe intensity continuity periodically (in regions where the fringe order changes). This discontinuity is very sensitive to the camera or projector defocusing blur, and therefore yields periodic phase error. These experimental results are consistent with previous analysis, demonstrating the settings in [35] and [36] would lead to suboptimal performance.

We further compare the performance with the traditional methods including Fourier transform profilometry [44], unwrapping methods with random speckle [31], triangular waves [33], and spatial constraints [10]. We set the frequency to 36 for all the fringes except for the spatial-constraint-based method, because the maximum depth range it can handle is  $\Delta Z_{\max} = \Delta y / \tan \theta$ , where  $\Delta y$  is the spatial span of one projected fringe period and  $\theta$  is the angle between projection and camera capture. In our system, the angle is approximately  $30^\circ$ , and therefore, we had to decrease the frequency to 12 for a higher depth range. We still use the three-frequency 32-step phase shift method as the benchmark and calculate the phase error.

Fig. 13 shows the experimental results, in which the first row are the captured fringes and the second row shows the measurement phase error. In Fig. 13(e), the spatial constraint method [10] works well in some regions; however, there are still some areas that exceed the maximum depth range and fail to be correctly unwrapped (the regions in red rectangles) even though the frequency was reduced to 12. Further decreasing the fringe frequency can increase the depth range; however,

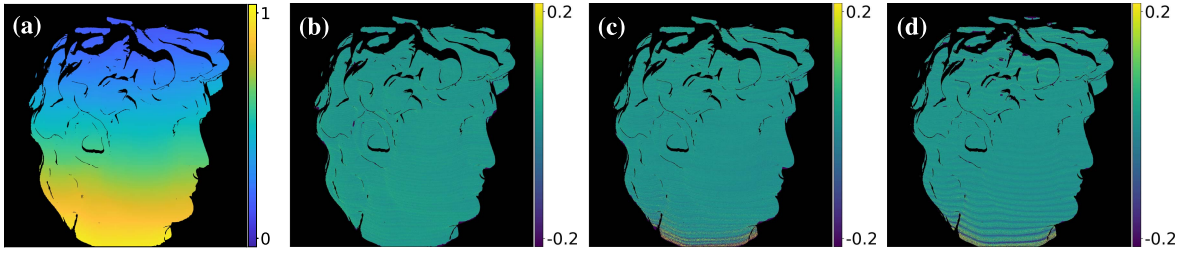


Fig. 11. Practical comparison. (a) Ideal absolute phase. (b) Phase error of the SUPS method. (c) and (d) Phase error of two embedding-based methods, respectively (see [36], [35]).

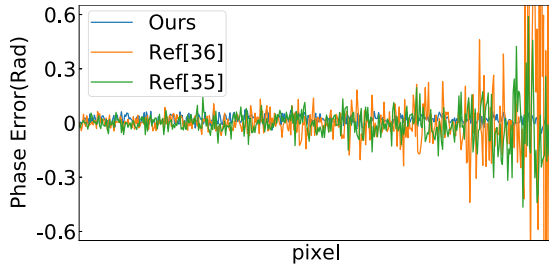


Fig. 12. Cross section of the phase error in Fig. 11(b)–(d).

the phase error would also increase. In Fig. 13(f) and (g), the PCPS method [33] and random speckle method [31] suffer from strip-like and speckle-distributed errors, respectively. The main reason for this phenomenon is the defocusing blur: the embedded discrete intensity signal destroys the fringe continuity, and hence is sensitive to defocusing. Fig. 14 reveals how optical defocusing affects the coding signal, where Fig. 14(a) shows the cross section of the coding fringe of the PCPS method, and Fig. 14(b) shows the cross section of the corresponding captured fringe. In the coding fringe, A and B have approximately the same intensity. However, affected by the neighbor pixels, the corresponding pixels A' and B' in the captured images have quite a large disparity, and these wrong pixel intensities eventually cause phase errors. Since A–B pairs periodically exist in the coding fringe, periodical phase error can be observed in Fig. 13(f). The Fourier transform profilometry method [44] fails to handle this sculpture with complex surface geometry, especially the hair part and the marginal regions as shown in Fig. 13(h). The result is consistent with the existing study [45] that the surface discontinuity and texture variation would introduce additional errors in phase extraction in the frequency domain. From these experimental results, our method achieves better performance and well addresses the conflict between accuracy and efficiency.

We then conducted comparative experiments with the Gray-code method [25], a representative phase unwrapping method using binary patterns. We adjust the fringe period to 32 pixels, and then the fringe frequency is  $1140/32 = 35.625$ . Since  $N$  Gray-code patterns can encode  $2^N$  fringe orders, the number of patterns required to encode the 36 fringe orders is 6 [ceil( $\log_2 36$ ), where the ceil( $\cdot$ ) function returns the round up value]. The experimental results are shown in Fig. 15. As shown in Fig. 15(d), the Gray-code method tends to suffer from a mismatch problem in the position where the fringe order changes, and the error pixels are marked with red color. The results are consistent with existing studies [6], [46] that

the boundary of the white and black fringe in the Gray-code images cannot be perfectly identified due to optical defocusing, hence introducing errors in the binarization process. Another noteworthy problem is that the Gray-code method requires additional patterns, and the number would increase with the fringe frequency, and therefore it is inefficient compared with our SUPS method.

In real-world 3-D shape measurements, the defocusing blur is hard to avoid due to the narrow DOF and rapid height changes in the measured object. The camera defocusing causes images blurred and the projector defocusing results in contrast decreases in fringes, and finally induces artifacts or empty zones in the reconstructed surfaces. To evaluate the defocusing robustness of the proposed method, we place the measured sculpture at different distances in front of the camera and keep other factors unchanged. The captured images are shown in the first row of Fig. 16, where the left one is in focus, and the right one is out of focus as approaching the camera. It can be clearly observed that as the object deviates from the best focus position, not only do the image details become blurred but also the contrast of the fringe projected decreases. The corresponding measurement results are shown in the bottom row of Fig. 16. As can be seen, despite the increase in defocusing, our algorithm can still obtain accurate results, which proves the defocusing robustness of the proposed method.

#### D. Discussion

The key idea of the proposed SUPS method is to internally embed an additional SPS that uniquely determines the fringe order information. This encoding strategy brings the following advantages.

- 1) *High Speed*: The proposed method recovers the absolute phase with fewer patterns than the conventional PMP methods, and the minimum number of patterns required is only four. Besides, the throughout pixelwise calculation pipeline is friendly to parallel computing devices such as GPUs. These factors contribute to higher efficiency and expand its application under dynamic conditions.
- 2) *High Accuracy*: By embedding fringe order information into the phase distribution, the proposed method preserves the fringe intensity modulation and is more robust to surface reflectivity variations or out-of-focus blur. Moreover, pixelwise calculation prevents error propagation from surrounding pixels. All these properties contribute to high accuracy.

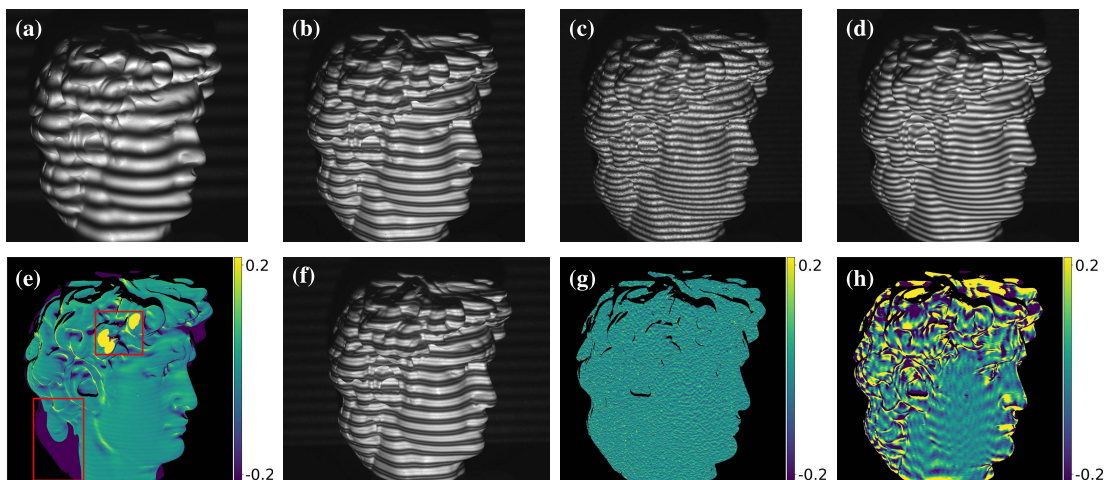


Fig. 13. Measurement result using existing methods. Captured fringes of (a) spatial-constraint-based method [10], (b) PCPS method [33], (c) speckle-based method [31], and (d) Fourier transform profilometry [44]. (e)–(h) Phase error corresponding to (a)–(d), respectively. (e) Regions in red rectangles exceed the maximum depth range and fail to be correctly unwrapped.

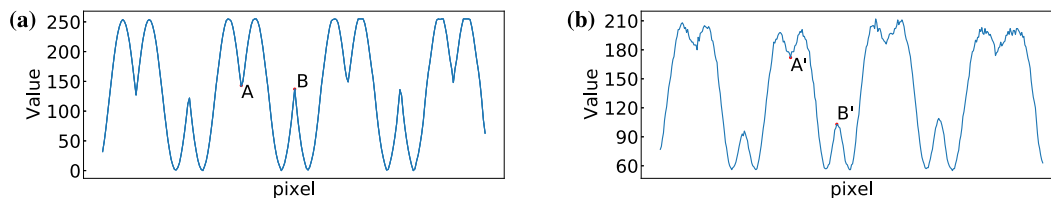


Fig. 14. Cross sections of (a) coding fringe and (b) its corresponding capture of PCPS method [33].

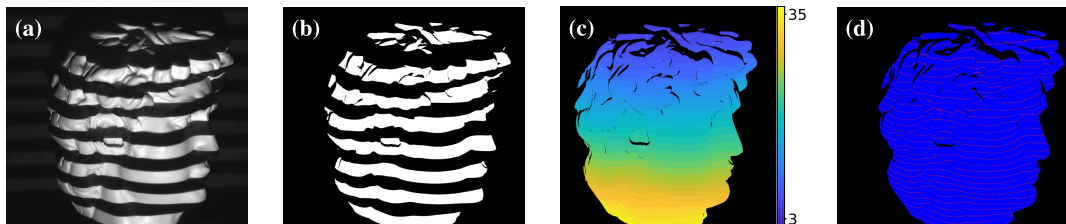


Fig. 15. Results of the Gray-code method. (a) Sixth (the densest) fringes. (b) Binarization result of (a). (c) Decoded fringe order. (d) Fringe order error (marked with red color).

3) *High Scalability*: Since many single-value functions are feasible for SPS theoretically (with a range less than  $2\pi$ ), our method has high scalability for further variants. Furthermore, it is easily deployed on the existing DLP systems without hardware adjustment.

The proposed SUPS method provides a promising solution to develop 3-D measurement systems with higher efficiency and accuracy. However, despite the great advantages mentioned above, there are some limitations that need to be considered. First, we mainly discuss and evaluate the case of linear and discrete staircase SPS in this article, but the optimal format is still an open question. The experimental comparison with some existing methods suggests that the SPS format also plays a great role in the measurement performance, so it deserves to be further studied what SPS should be selected. Second, the median filtering operation is applied in the SPS extraction procedure to remove some noise. Though simple and effective, these operations on neighboring pixels may introduce artifacts in the absolute phase map when measuring surfaces with large height differences. Further studies will focus on developing error self-correction techniques for the SUPS method by introducing the correspondence between the

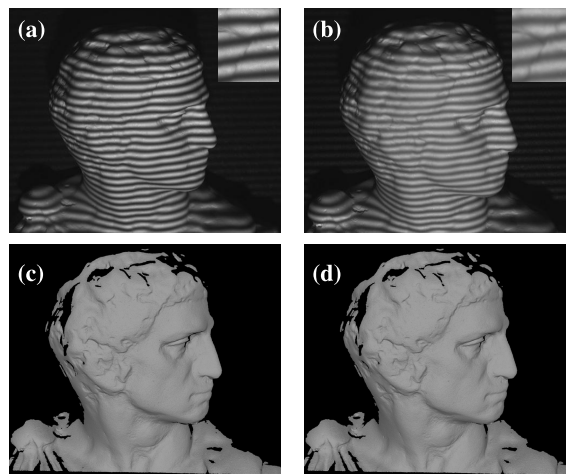


Fig. 16. Defocusing measurement results. (a) In-focus fringe image. (b) Out-of-focus fringe image. Note the top-right enlarged views show the fringe blur caused by defocusing. (c) Reconstructed surface from (a). (d) Reconstructed surface from (b).

SPS and the wrapped phase, the monotonicity constraints of the phase map.

## V. CONCLUSION

In this article, we propose a generic multistep SUPS method that requires no additional patterns or postprocessing for phase unwrapping. The main idea is to introduce a novel SPS into sinusoidal patterns and recover the absolute phase without external information. This strategy leads to several advantages. First, it prevents redundant pattern projections for higher efficiency and enables absolute phase retrieval through at least four patterns. Second, the embedded phase shift preserves the fringe intensity modulation and thus achieves high accuracy. Furthermore, the throughout calculation process is pixelwise and hence friendly to parallel computing devices.

We verify its superiority in accuracy and efficiency through extensive theoretical analysis, simulations, and experiments. The experimental results on a standard plane and several representative sculptures demonstrate its feasibility on real-world surfaces with complex geometry and out-of-focus blur. With high scalability, our study provides a theoretical framework for future studies to develop and assess self-unwrapping methods based on phase-embedding. Future research will focus on performance improvement, including exploring fringe frequency strategy and the optimal SPS format.

## REFERENCES

- [1] R. Anchini, G. D. Leo, C. Liguori, and A. Paolillo, "A new calibration procedure for 3-D shape measurement system based on phase-shifting projected fringe profilometry," *IEEE Trans. Instrum. Meas.*, vol. 58, no. 5, pp. 1291–1298, May 2009.
- [2] J. Salvi, S. Fernandez, T. Pribanic, and X. Llado, "A state of the art in structured light patterns for surface profilometry," *Pattern Recognit.*, vol. 43, no. 8, pp. 2666–2680, Aug. 2010.
- [3] Y. Hu, J. Xi, Z. Yang, J. F. Chicharo, W. Cheng, and Z. Yang, "Inverse function analysis method for fringe pattern profilometry," *IEEE Trans. Instrum. Meas.*, vol. 58, no. 9, pp. 3305–3314, Sep. 2009.
- [4] M. Duan, Y. Jin, H. Chen, J. Zheng, C. Zhu, and E. Chen, "Automatic 3-D measurement method for nonuniform moving objects," *IEEE Trans. Instrum. Meas.*, vol. 70, pp. 1–11, 2021.
- [5] X.-Y. Su, W. Zhou, G. von Bally, and D. Vukicevic, "Automated phase-measuring profilometry using defocused projection of a Ronchi grating," *Opt. Commun.*, vol. 94, no. 6, pp. 561–573, 1992.
- [6] C. Zuo, L. Huang, M. Zhang, Q. Chen, and A. Asundi, "Temporal phase unwrapping algorithms for fringe projection profilometry: A comparative review," *Opt. Lasers Eng.*, vol. 85, pp. 84–103, Oct. 2016.
- [7] H. Yu, Y. Lan, Z. Yuan, J. Xu, and H. Lee, "Phase unwrapping in InSAR: A review," *IEEE Geosci. Remote Sens. Mag.*, vol. 7, no. 1, pp. 40–58, Mar. 2019.
- [8] J.-S. Hyun and S. Zhang, "High-speed three-dimensional absolute shape measurement with three projected binary patterns," *Opt. Eng.*, vol. 59, no. 2, Feb. 2020, Art. no. 024104.
- [9] F. Da, X. Wang, and H. Huang, "Phase unwrapping using interlaced fringes for phase-shifting techniques," *IEEE Trans. Instrum. Meas.*, vol. 60, no. 9, pp. 3185–3193, Sep. 2011.
- [10] Y. T. An, J. S. Hyun, and S. Zhang, "Pixel-wise absolute phase unwrapping using geometric constraints of structured light system," *Opt. Exp.*, vol. 24, no. 16, pp. 18445–18459, 2016.
- [11] S. Zhang, "Absolute phase retrieval methods for digital fringe projection profilometry: A review," *Opt. Lasers Eng.*, vol. 107, pp. 28–37, Aug. 2018.
- [12] C. Lin, D. Zheng, Q. Kemao, J. Han, and L. Bai, "Spatial pattern-shifting method for complete two-wavelength fringe projection profilometry," *Opt. Lett.*, vol. 45, no. 11, pp. 3115–3118, 2020.
- [13] I. Gurov and M. Volkov, "Fringe evaluation and phase unwrapping of complicated fringe patterns by the data-dependent fringe processing method," *IEEE Trans. Instrum. Meas.*, vol. 55, no. 5, pp. 1634–1640, Oct. 2006.
- [14] K. Chen, J. Xi, and Y. Yu, "Quality-guided spatial phase unwrapping algorithm for fast three-dimensional measurement," *Opt. Commun.*, vol. 294, pp. 139–147, May 2013.
- [15] C. W. Chen and H. A. Zebker, "Two-dimensional phase unwrapping with use of statistical models for cost functions in nonlinear optimization," *J. Opt. Soc. Amer. A, Opt. Image Sci.*, vol. 18, no. 2, pp. 338–351, 2001.
- [16] Q. Kemao, "Windowed Fourier transform for fringe pattern analysis," *Appl. Opt.*, vol. 43, no. 13, pp. 2695–2702, 2004.
- [17] F. Da and H. Huang, "A fast, accurate phase unwrapping method for wavelet-transform profilometry," *Opt. Commun.*, vol. 285, no. 4, pp. 421–432, Feb. 2012.
- [18] S. Zhang, *High-Speed 3D Imaging With Digital Fringe Projection Techniques*. Boca Raton, FL, USA: CRC Press, 2018.
- [19] A. G. Marrugo, F. Gao, and S. Zhang, "State-of-the-art active optical techniques for three-dimensional surface metrology: A review [invited]," *J. Opt. Soc. Amer. A, Opt. Image Sci.*, vol. 37, no. 9, p. B60, 2020.
- [20] Y.-Y. Cheng and J. C. Wyant, "Multiple-wavelength phase-shifting interferometry," *Appl. Opt.*, vol. 24, no. 6, pp. 804–807, 1985.
- [21] X. Peng, Z. Yang, and H. Niu, "Multi-resolution reconstruction of 3-D image with modified temporal unwrapping algorithm," *Opt. Commun.*, vol. 224, nos. 1–3, pp. 35–44, Aug. 2003.
- [22] Z. Wang, D. A. Nguyen, and J. C. Barnes, "Some practical considerations in fringe projection profilometry," *Opt. Lasers Eng.*, vol. 48, no. 2, pp. 218–225, Feb. 2010.
- [23] Y. Ding, J. Xi, Y. Yu, W. Cheng, S. Wang, and J. F. Chicharo, "Frequency selection in absolute phase maps recovery with two frequency projection fringes," *Opt. Exp.*, vol. 20, no. 12, pp. 13238–13251, Jun. 2012.
- [24] W. Yin *et al.*, "High-speed three-dimensional shape measurement using geometry-constraint-based number-theoretical phase unwrapping," *Opt. Lasers Eng.*, vol. 115, pp. 21–31, Apr. 2019.
- [25] G. Sansoni, M. Carocci, and R. Rodella, "Three-dimensional vision based on a combination of gray-code and phase-shift light projection: Analysis and compensation of the systematic errors," *Appl. Opt.*, vol. 38, no. 31, pp. 6565–6573, Nov. 1999.
- [26] X. Chen, C. Lu, M. Ma, X. Mao, and T. Mei, "Color-coding and phase-shift method for absolute phase measurement," *Opt. Commun.*, vols. 298–299, pp. 54–58, Jul. 2013.
- [27] Y. Wang and S. Zhang, "Novel phase-coding method for absolute phase retrieval," *Opt. Lett.*, vol. 37, no. 11, pp. 2067–2069, 2012.
- [28] D. Zheng and F. Da, "Phase coding method for absolute phase retrieval with a large number of codewords," *Opt. Exp.*, vol. 20, no. 22, pp. 24139–24150, 2012.
- [29] X. Chen *et al.*, "Two-digit phase-coding strategy for fringe projection profilometry," *IEEE Trans. Instrum. Meas.*, vol. 70, pp. 1–9, 2021.
- [30] Y. Zhang, Z. Xiong, Z. Yang, and F. Wu, "Real-time scalable depth sensing with hybrid structured light illumination," *IEEE Trans. Image Process.*, vol. 23, no. 1, pp. 97–109, Jan. 2014.
- [31] Y. Zhang, Z. Xiong, and F. Wu, "Unambiguous 3D measurement from speckle-embedded fringe," *Appl. Opt.*, vol. 52, no. 32, pp. 7797–7805, 2013.
- [32] W. Lohry, V. Chen, and S. Zhang, "Absolute three-dimensional shape measurement using coded fringe patterns without phase unwrapping or projector calibration," *Opt. Exp.*, vol. 22, no. 2, pp. 1287–1301, 2014.
- [33] Y. Wang, K. Liu, Q. Hao, D. L. Lau, and L. G. Hassebrook, "Period coded phase shifting strategy for real-time 3-D structured light illumination," *IEEE Trans. Image Process.*, vol. 20, no. 11, pp. 3001–3013, Nov. 2011.
- [34] C. Zuo, S. Feng, L. Huang, T. Tao, W. Yin, and Q. Chen, "Phase shifting algorithms for fringe projection profilometry: A review," *Opt. Lasers Eng.*, vol. 109, pp. 23–59, Oct. 2018.
- [35] G. Wu, Y. Wu, L. Li, and F. Liu, "High-resolution few-pattern method for 3D optical measurement," *Opt. Lett.*, vol. 44, no. 14, pp. 3602–3605, Jul. 2019.
- [36] Y. Wu *et al.*, "Inner shifting-phase method for high-speed high-resolution 3-D measurement," *IEEE Trans. Instrum. Meas.*, vol. 69, no. 9, pp. 7233–7239, Sep. 2020.
- [37] K. He, X. Zhang, S. Ren, and J. Sun, "Deep residual learning for image recognition," in *Proc. IEEE Conf. Comput. Vis. Pattern Recognit. (CVPR)*, Jun. 2016, pp. 770–778.
- [38] S. Van der Jeught and J. J. Dirckx, "Deep neural networks for single shot structured light profilometry," *Opt. Exp.*, vol. 27, no. 12, pp. 17091–17101, 2019.
- [39] K. Wang, Y. Li, Q. Kemao, J. Di, and J. Zhao, "One-step robust deep learning phase unwrapping," *Opt. Exp.*, vol. 27, no. 10, pp. 15100–15115, 2019.
- [40] S. Feng *et al.*, "Fringe pattern analysis using deep learning," *Adv. Photon.*, vol. 1, no. 2, Feb. 2019, Art. no. 025001.

- [41] J. Qian *et al.*, "Deep-learning-enabled geometric constraints and phase unwrapping for single-shot absolute 3D shape measurement," *APL Photon.*, vol. 5, no. 4, Apr. 2020, Art. no. 046105.
- [42] Z. Zhang, "A flexible new technique for camera calibration," *IEEE Trans. Pattern Anal. Mach. Intell.*, vol. 22, no. 11, pp. 1330–1334, Nov. 2000.
- [43] P. Cignoni, M. Callieri, M. Corsini, M. Dellepiane, F. Ganovelli, and G. Ranzuglia, "Meshlab: An open-source mesh processing tool," in *Proc. Eurograph. Italian Chapter Conf.*, 2008, pp. 129–136.
- [44] M. Takeda and K. Mutoh, "Fourier transform profilometry for the automatic measurement of 3-D object shapes," *Appl. Opt.*, vol. 22, no. 24, pp. 3977–3982, 1983.
- [45] L. Huang, Q. Kema, B. Pan, and A. K. Asundi, "Comparison of Fourier transform, windowed Fourier transform, and wavelet transform methods for phase extraction from a single fringe pattern in fringe projection profilometry," *Opt. Lasers Eng.*, vol. 48, no. 2, pp. 141–148, Feb. 2010.
- [46] D. Zheng and F. Da, "Self-correction phase unwrapping method based on gray-code light," *Opt. Lasers Eng.*, vol. 50, no. 8, pp. 1130–1139, Aug. 2012.



**Jinghui Zeng** received the B.S. degree in optoelectronic information science and engineering from the South China University of Technology, Guangzhou, China, in 2017, where he is currently pursuing the Ph.D. degree in software engineering with the Shien-Ming Wu School of Intelligent Engineering.

His current research interests include computer vision, structured light 3-D measurement, and surface reconstruction.



**Wenxin Ma** received the B.S. degree in information engineering and the M.S. degree in software engineering from the South China University of Technology, Guangzhou, China, in 2018 and 2021, respectively.

His research interests include deep learning, 3-D object detection, and phase unwrapping.



**Wei Jia** received the bachelor's degree from Harbin Engineering University, Harbin, China, in 2004, the master's degree from the University of Bristol, Bristol, U.K., in 2006, and the Ph.D. degree from Dundee University, Dundee, U.K., in 2012, all in computer science.

She is currently a Senior Researcher with Guangzhou Shiyuan Electronic Technology Company, Ltd., (CVTE) Research, Guangzhou, China. She also leads a 3-D Vision Group. Her current research interests include 3-D imaging, 3-D reconstruction, neural networks, and deep learning.



**Yucheng Li** received the B.S. degree in measurement and control technology and instrument from Xiangtan University, Xiangtan, China, in 2017, and the M.S. degree in control science and engineering from Hunan University, Changsha, China, in 2020.

His current research interests include structured light, surface reconstruction, and high-performance computing.



**Haowen Li** received the B.S. degree in automation and the M.S. degree in control science and engineering from Hunan University, Changsha, China, in 2018 and 2021, respectively.

His research interests include 3-D measurement and machine vision.



**Xuewen Liu** received the B.S. degree in automation and the M.S. degree in control science and engineering from Hunan University, Changsha, China, in 2018 and 2021, respectively.

His research interests include 3-D measurement and machine vision.



**Mingkui Tan** (Member, IEEE) received the bachelor's degree in environmental science and engineering and the master's degree in control science and engineering from Hunan University, Changsha, China, in 2006 and 2009, respectively, and the Ph.D. degree in computer science from Nanyang Technological University, Singapore, in 2014.

From 2014 to 2016, he was a Senior Research Associate in computer vision with the School of Computer Science, The University of Adelaide, Adelaide, SA, Australia. He is currently a Professor with the School of Software Engineering, South China University of Technology, Guangzhou, China. His research interests include machine learning, sparse analysis, deep learning, and large-scale optimization.